



MEG-based detection and localization of perilesional dysfunction in chronic stroke



Ron K.O. Chu^{a,c,*}, Allen R. Braun^e, Jed A. Meltzer^{a,b,c,d}

^aUniversity of Toronto, Department of Psychology, 100 St. George Street, 4th Floor, Sidney Smith Hall, Toronto, ON M5S 3G3, Canada

^bUniversity of Toronto, Department of Speech-Language Pathology, 160-500 University Avenue, Toronto, ON M5G 1V7, Canada

^cRotman Research Institute, Baycrest Centre, 3560 Bathurst St., Toronto, ON M6A 2E1, Canada

^dHeart and Stroke Foundation Canadian Partnership for Stroke Recovery, 600 Peter Morand Cres., Suite 201, Ottawa, ON K1G 5Z3, Canada

^eLanguage Section, National Institute on Deafness and Other Communication Disorders, National Institutes of Health, Bethesda, MD, USA

ARTICLE INFO

Article history:

Received 13 November 2014

Received in revised form 20 March 2015

Accepted 23 March 2015

Available online 8 April 2015

Keywords:

Magnetoencephalography
Beamformer source reconstruction
Time–frequency analysis
Chronic stroke

ABSTRACT

Post-stroke impairment is associated not only with structural lesions, but also with dysfunction in surviving perilesional tissue. Previous studies using equivalent current dipole source localization of MEG/EEG signals have demonstrated a preponderance of slow-wave activity localized to perilesional areas. Recent studies have also demonstrated the utility of nonlinear analyses such as multiscale entropy (MSE) for quantifying neuronal dysfunction in a wide range of pathologies. The current study utilized beamformer-based reconstruction of signals in source space to compare spectral and nonlinear measures of electrical activity in perilesional and healthy cortices. Data were collected from chronic stroke patients and healthy controls, both young and elderly. We assessed relative power in the delta (1–4 Hz), theta (4–7 Hz), alpha (8–12 Hz) and beta (15–30 Hz) frequency bands, and also measured the nonlinear complexity of electrical activity using MSE. Perilesional tissue exhibited a general slowing of the power spectrum (increased delta/theta, decreased beta) as well as a reduction in MSE. All measures tested were similarly sensitive to changes in the posterior perilesional regions, but anterior perilesional dysfunction was detected better by MSE and beta power. The findings also suggest that MSE is specifically sensitive to electrophysiological dysfunction in perilesional tissue, while spectral measures were additionally affected by an increase in rolandic beta power with advanced age. Furthermore, perilesional electrophysiological abnormalities in the left hemisphere were correlated with the degree of language task-induced activation in the right hemisphere. Finally, we demonstrate that single subject spectral and nonlinear analyses can identify dysfunctional perilesional regions within individual patients that may be ideal targets for interventions with non-invasive brain stimulation.

© 2015 The Authors. Published by Elsevier Inc. This is an open access article under the CC BY license (<http://creativecommons.org/licenses/by/4.0/>).

1. Introduction

Stroke causes profound disturbances to cognition, and is a leading cause of adult disability. One of the most debilitating cognitive impairments is aphasia, which typically occurs following damage to language networks in the left hemisphere. As stroke-induced cortical lesions are essentially permanent, language recovery is thought to proceed from processes of reorganization and neural plasticity occurring in structurally intact brain tissue. Specifically, reorganization of the language network after stroke is associated with the recruitment of structurally intact, perilesional tissue (Cornelissen et al., 2003; Warburton et al., 1999) and contralateral homotopic language areas (Musso et al., 1999; Thulborn et al., 1999; Tillema et al., 2008). Although both perilesional

and contralesional activities are thought to play a role in recovery, recruitment of perilesional areas is associated with a better long-term outcome (Heiss and Thiel, 2006), and a shift from right to left hemisphere activation has been observed to occur during spontaneous recovery (Saur et al., 2006) and with treatment (Wilson et al., 2012). With the advent of noninvasive brain stimulation as a viable treatment for aphasia and post-stroke motor disorders, positive results have been obtained from efforts to induce a shift from contralesional to perilesional activity, either through excitatory stimulation of the affected hemisphere or through inhibition of the unaffected hemisphere (Kang et al., 2011; Marangolo et al., 2013; Naeser et al., 2005a; Szaflarski et al., 2011). It is still unknown why perilesional tissue remains underactivated in some patients. In some cases, patients may have large lesions that engulf most of the left hemisphere language areas; as such, language processing must be relegated to right hemisphere homologues. However in other cases, perilesional tissue may be structurally intact, but ‘functionally lesioned’ (Hofmeijer and van Putten, 2012) representing an ideal

* Corresponding author at: 3560 Bathurst St., Toronto, ON, Canada. Tel.: +1 416 785 2500x2117.

E-mail address: ron.chu@utoronto.ca (R.K.O. Chu).

target for intervention. Therefore, noninvasive methods to identify functional abnormalities in the perilesional tissue will help guide physiological interventions to target the most relevant areas, and to assess their effectiveness. The current study demonstrates that spectral and nonlinear analyses of source localized MEG signals can be used to identify dysfunctional perilesional tissue.

One of the most prominent indices of tissue dysfunction following stroke is a change in spontaneous oscillatory activity measured by spectral analyses of MEG/EEG signals. Studies have found increased low frequency (Butz et al., 2004; Harmony et al., 1995; Machado et al., 2004; Meinzer et al., 2013; Zappasodi et al., 2007) and attenuated high frequency (Cuspineda et al., 2009) spontaneous activity, localized to the perilesional areas. Importantly, improved functional outcomes are associated with a reduction in perilesional low frequency amplification (Meinzer et al., 2004, 2008; Zappasodi et al., 2007) and an increase in perilesional alpha-band functional connectivity (Westlake et al., 2012). Thus, low frequency amplification and high frequency attenuation are promising indicators of dysfunctional perilesional tissue.

Although most characterizations of pathological spontaneous activity in stroke have centered on spectral analyses, researchers have also applied techniques from the field of nonlinear dynamics towards analysis of brain signals in other disorders (for a review, see Stam, 2005). In particular, measures based on the concept of entropy have been especially useful. The various algorithms incorporating this term aim for a measure of the complexity of neural dynamics, with complexity indicating a rich temporal structure that is neither random (e.g., white noise) nor strictly periodic. In this study, we examine multiscale entropy (MSE; Costa et al., 2002, 2005), an increasingly popular technique that assesses time series complexity across multiple time scales, reducing the arbitrariness inherent in pre-selecting a specific time scale (see the Methods section for details). Reduced MSE has recently been demonstrated in brain injury (Raja Beharelle et al., 2012), autism (Bosl et al., 2011; Catarino et al., 2011) and Alzheimer's disease (Hornero et al., 2008; Park et al., 2007).

Given the success of MSE to characterize dysfunctional physiological signals, the current study aimed to compare MSE with the more traditional measures of spectral power in their ability to characterize perilesional dysfunction. We used beamforming analysis of MEG data to localize and quantify abnormal perilesional activity in patients who have had a stroke in the left hemisphere of the brain. The patients were participating in a MEG study of language processing, aiming to identify networks that are recruited to support language comprehension in post-stroke aphasia (Meltzer et al., 2013). In the present study, we analyzed spontaneous aspects of the MEG data collected from these patients, focusing on the intertrial interval of the language comprehension task, but obtaining very similar results from data extracted from the task periods. We hypothesized that, irrespective of engagement in a cognitive task, altered neural dynamics would be present in the perilesional tissue, compared to other brain regions and compared to the same brain regions in healthy control participants. We used both spectral-based and entropy-based measurements, and report here the similarities and differences found in these approaches. Specifically, the measures were compared along two levels: 1) the spatial extent of abnormal spontaneous activity detected by these measures and 2) the degree to which spontaneous perilesional activity predicted language activation in the right hemisphere homologues, a frequently observed consequence of damage or dysfunction in the left hemisphere language areas (Crinion and Price, 2005; Saur et al., 2006; Thompson and den Ouden, 2008).

The above questions were addressed with five different analyses. To address the first question, we 1) computed voxel-based comparisons of source localized relative power and MSE between patients and controls. To illustrate the differences in power spectra that drove the differences between groups seen in the whole-brain maps, we 2) additionally computed power spectra in selected regions of interest (ROIs). To address

the second question, we 3) computed task activation maps and 4) assessed correlations between task activation in the right hemisphere and characteristics of spontaneous signals in the left hemisphere. Finally, we 5) computed single subject maps to demonstrate the clinical utility of this approach for detecting tissue dysfunction within individual patients. Additionally, to further characterize the relationships between the nonlinear and spectral measures, we examined across-subjects correlations between MSE and relative power in different bands.

2. Methods

2.1. Participants

MEG data were obtained from three groups of participants, who had participated in studies of language comprehension (Meltzer et al., 2013; Meltzer and Braun, 2011). These included 25 patients (11 female, 2 left-handed) with aphasia, resulting from a single left-hemisphere ischemic stroke which occurred at least 6 months prior to testing (0.7–24.3 years, mean 5.8 years). Patients ranged in age from 34–72 years (mean 57). The study was approved by the Institutional Review Board of the NIH Intramural Program (NIH protocol 92-DC-0178). The participants were financially compensated.

Imaging data from aphasic participants were compared with data from two control groups. First, there was a young control group, consisting of 24 healthy subjects (12 female, aged 22–37, mean 27). Additionally, to control for the effects of aging, we recruited an older control group, consisting of nine healthy subjects matched in age to the aphasic patients (range 44–71, mean 53). All young and age-matched controls were right-handed. None of the participants reported any developmental language difficulties.

The aphasic patients and the older control subjects underwent an extensive battery of cognitive and neurolinguistic assessments in addition to MEG and structural MRI, while the younger controls only completed the neuroimaging components. All older control subjects tested were within the normal limits on all cognitive and linguistic tests, while the aphasic patients exhibited deficits consistent with their diagnosis of post-stroke aphasia. More details regarding the lesion characteristics and neuropsychological profiles of the patients can be found in Meltzer et al. (2013).

The smaller number of age-matched controls reduced the power of our contrasts to reveal aging-related changes. However, as demonstrated in the results, both young and age-matched controls demonstrated comparable differences relative to aphasic patients, localized to the perilesional regions, although the effects were stronger for young controls. Critically, the age-matched controls served to confirm that the current findings were related to stroke and not aging.

2.2. Sentence picture-matching paradigm

The participants performed a sentence picture-matching task during MEG scanning. Complete details of the sentence and picture materials can be found in previous reports (Meltzer et al., 2013; Meltzer and Braun, 2011). A brief description of the paradigm is as follows. On each trial, subjects heard a sentence, spoken at a natural rate, while viewing a fixation cross. After the sentence, the fixation cross remained during a 3-s memory delay. Next, the cross was replaced by two pictures. Subjects indicated which picture correctly depicted the action described in the sentence, by pressing the left or right button on a fiber optic response box. Pictures remained on screen for 4 s, and were followed by an inter-trial interval of 2.1–2.25 s. Trials were presented in seven runs of 36 trials each, and subjects were allowed to rest in between runs if desired. The total time for the experiment was approximately 1 h and 30 min, including preparation.

Triggers were inserted into the MEG acquisition stream to allow for analysis of the MEG signal during each time period of the task. In the

present study, we assessed spontaneous aspects of perilesional neural activity by analyzing data from the intertrial interval, using data epochs consisting of 1 s prior to sentence onset. Thus, analyses are based on 252 1-s epochs per participant. Data from the intertrial interval reflect a state of seated relaxation but high alertness, as participants were engaged in a cognitive task but were not actively processing sensory or cognitive information at the time. The possible implications of this selection of data as opposed to “true rest” are addressed in the Discussion section.

2.3. Anatomical MRI

Each patient underwent an anatomical MRI session, for purposes of MEG source localization and lesion delineation. MRI was acquired on a General Electric, Signa 3-Tesla scanner with an 8-channel head coil, using parallel imaging with ASSET reconstruction. Scans included a T1-weighted 3D high-resolution MPRAGE (1 mm isotropic resolution, Fast Spin-echo T2, T2 and FLAIR (both 3.5 mm thick slices)). T1 images were skull stripped by applying a stripping procedure to the T2-weighted image, applying the resulting mask to the T1 image, and making further manual adjustments. This procedure produces better results than stripping the T1 image directly, due to the presence of large lesions that appear dark on T1 contrast.

Lesion borders were delineated using segmentation tools in FSL and ROI drawing tools in AFNI, based on a T1 intensity threshold followed by manual adjustments. Regions of gliosis were included in the lesion on the basis of hyperintense signal seen in a coregistered T2–FLAIR image. T1 images were spatially normalized by computing a 12-parameter affine registration between the individual patient brains and the “Colin brain” in Talairach space. Nonlinear registration algorithms produced slightly better registrations in some cases, but were not reliable for all patients in the presence of large lesions, so affine registration was adapted for consistency across the cohort. Cost-function masking was applied using the individual lesion masks to exclude the lesioned area from the warp computation. Using the computed affine matrices, both T1 anatomical images and lesion masks were warped into Talairach space for group analysis of lesion characteristics and source-localized MEG activation.

For the display of activation maps derived from patient data, we constructed a “composite lesion underlay” to indicate damaged regions with the greatest overlap across patients. The spatially normalized T1-weighted anatomical images of the 25 patients were averaged together. The resulting image was further darkened by subtracting a percentage of the signal proportional to the number of patients having a lesion at each voxel.

2.4. MEG acquisition and analysis

MEG was recorded with a CTF Omega 2000 system, comprising 275 first order axial gradiometers. For environmental noise reduction, synthetic third-order gradiometer signals were obtained through adaptive subtraction of 33 reference channels located inside the MEG dewar far from the head. Signals were digitized at 600 Hz with an anti-aliasing filter at 125 Hz. Head position was tracked continuously using coils placed at three fiducial points on the head (McCubbin et al., 2004, 2004). The average head position over the entire experiment was used for source localization, and coregistered with the same fiducial points marked on the anatomical MRI using adhesive marker disks. In no cases did the total root-mean-square of movement for any coil exceed 1 cm.

2.5. Synthetic aperture magnetometry

MEG source analysis was conducted using synthetic aperture magnetometry (SAM) (Vrba and Robinson, 2001), as implemented in CTF software (CTF, Port Coquitlam, British Columbia, Canada). SAM is a beamformer technique that can be used to compute the full time course

of virtual channels at selected individual locations, or on a regular grid of locations (voxels) spread across the brain. SAM is a scalar beamformer, in which a nonlinear optimization technique is used to select one direction of current flow at each voxel to maximize dipole power. In short, SAM provides a series of weights for each voxel; the weights are computed so as to pass signal from a dipole located in the target voxel, while minimizing signal power from all other locations. We computed weights on a whole-brain grid of locations spaced 1 cm apart. These weights were then multiplied with the original sensor time series data to yield a new, spatially filtered, time series signal at each voxel (1 cm³). Normalized weights were used to render virtual signals in dimensionless units of signal-to-noise ratio, with noise power estimated as the lowest singular value of the sensor covariance matrix (Vrba and Robinson, 2001). This weight normalization step is commonly used to compensate for the depth-bias inherent in beamforming. However, because all our analyses are scaled to the signal strength, this step does not affect the results of the study at all. Signals were filtered at 0–80 Hz prior to beamforming.

2.6. Exploratory analysis of perilesional abnormalities

As mentioned above, we are presenting a reanalysis of data from an experiment originally designed to assess adaptive right hemisphere activation in aphasia (Meltzer et al., 2013). The present study evaluates new methods for characterizing abnormal spontaneous activity in perilesional tissue in stroke patients. Although all statistical maps are corrected for multiple comparisons across voxels, we did not conduct additional correction across the multiple signal quantities (e.g., relative delta power, theta power and multiscale entropy) assessed in this study. As such, the following analyses are exploratory in nature, and the methods identified as being the most sensitive and specific may be used in future confirmatory studies in which study design and statistical power are optimized to test specific hypotheses about perilesional electrophysiological abnormalities, such as their relationship to other indices of pathology (e.g., blood flow, metabolism, white matter disconnection).

2.6.1. SAM maps — spontaneous activity during the intertrial interval

We tested for changes in the frequency content of spontaneous MEG signals using spectral analysis. At each voxel, the power spectrum of the virtual signal for each data epoch was computed using Welch’s method in Matlab (Fast Fourier Transform of 500 ms Hamming windows with 50% overlap). Power spectra were averaged across epochs.

To evaluate quantitative parameters related to slowing of spontaneous activity, we computed measures of relative power from the resulting power spectra. Relative power of the delta (1–4 Hz), theta (4–7 Hz), alpha (8–12 Hz) and beta (15–30 Hz) frequency bands were calculated as the ratio of the power of each specific frequency band divided by the total power across 0–80 Hz. Computing relative power over the frequency spectrum avoids potential confounds introduced by the normalized beamformer weights (Luckhoo et al., 2014) and effectively bases the analysis on spectral shape rather than levels of absolute power.

Besides measures based on the power spectrum, we also calculated MSE from the time series signal at each voxel; a detailed explanation of MSE calculations can be found in Costa et al. (2002). MSE is an increasingly popular technique from a family of techniques that have included approximate entropy (ApEn), introduced by Pincus (1991), and the later refinement sample entropy (SampEn; Richman and Moorman, 2000). Most entropy estimation methods are dependent on a choice of parameters, the most critical of which is the time scale on which successive samples are compared. MSE addresses the problem of time scale selection by successively averaging the signal across progressively larger scales, and computing SampEn at each scale, denoted by a scaling parameter. The original sampled time series is generally

the finest time scale, while increasingly coarser scales are obtained by averaging successive values. Sample entropy is the negative natural logarithm of the conditional probability that two sequences of m consecutive data points, within a tolerance r , will remain similar following the addition of the next consecutive data point. The tolerance value r is a threshold for a binarized decision on whether two sequences are sufficiently similar to constitute a “match,” and is commonly scaled by the standard deviation of the time series. Put simply, lower values of SampEn indicate time series that have more self-similarity: the shape of successive values centered around one time resembles that centered around other times. Both periodic and completely random signals (e.g., white noise) are low in sample entropy, while complex aperiodic signals (e.g., $1/f$ noise) are higher in sample entropy (Costa et al., 2005, 2002).

Sample entropy was calculated with the parameters $m = 2$ and $r = 0.2$ from scales 1–12, which corresponded to time scales of approximately 1.5–20 ms. The entropy values averaged across the 12 time scales were used for the MSE maps. There are no clear guidelines for choosing parameter values, though r values typically range between 0.1 and 0.25 and m values are either 1 or 2 (see Lake et al., 2002 for a discussion of the optimal choices for m and r).

These methods produced whole-brain 3D-maps (including the infarcted regions) of relative power in each frequency band, and MSE. The maps were then warped into Talairach space by applying the transformation computed on anatomical images (see above), and interpolated to a final resolution of 5 mm³. The maps for patients and controls were compared using voxel-wise independent sample t -tests implemented in AFNI. All of the maps were thresholded at $p < 0.005$, with a minimum cluster size of 10 voxels to keep the family-wise error rate at $p < 0.05$. This threshold was based on Monte Carlo simulations from the 3dClustSim tool in AFNI using an FWHM of 8, as calculated previously with the same data (Meltzer et al., 2013).

2.6.2. SAM maps – task activation

The SAM technique can also be used to map task-related neural activity using a pseudo- T statistic, which is a normalized measure of the difference in oscillatory power in a given frequency range between two time windows (Vrba and Robinson, 2001). Previous results have demonstrated that task-induced neural activity generally results in decreased oscillatory power in the 8–30 Hz range, both in simple sensory and complex cognitive paradigms (Brookes et al., 2005; Hillebrand et al., 2005; Singh et al., 2002). Thus, we created single subject, pseudo- T SAM maps which quantified the change in 8–30 Hz power between the sentence listening period and the baseline intertrial interval. The values from these pseudo- T maps were subjected to group level analysis to assess neural activity related to sentence processing between patients and controls, as well as ROI analyses in patients to assess the correlation between perilesional spontaneous activities and task-induced activation of the homologous contralesional cortex.

2.6.3. ROI analyses

Voxel-wise statistical maps provide a good overview of differences between patients and controls, but are potentially affected by variability in the lesion extent across patients. To directly test the hypothesis that perilesional regions generate abnormal physiological activity, we analyzed changes in relative band power and MSE within specific regions of interest in both hemispheres.

To quantitatively assess the degree of dysfunction detected by the spectral and nonlinear measures we selected two atlas-based regions that consistently tended to border the anterior and posterior portions of lesions in most of the patients. To do so, we visually inspected the map of lesion overlap (see Meltzer et al., 2013, Fig. 4a), and compared it with an atlas of 90 macroanatomical regions (Eickhoff et al., 2005). From this inspection we identified the middle frontal gyrus as an ideal anterior ROI. Two regions from that atlas, labeled as “angular gyrus” and “inferior parietal lobe,” were combined into a posterior ROI in each hemisphere. In each patient, the ROI was masked by the lesion

maps in order to exclude lesioned voxels. On average, 22.67% (SD = 25) of the posterior ROI and 19.15% (SD = 19.46) of the anterior ROI were excluded due to lesion overlap.

The atlas-based ROIs provide a means to assess signal characteristics in consistent locations across subjects, but they are not truly “perilesional” in all subjects due to variability in lesion location and extent. Therefore, we also constructed customized perilesional and contralesional ROIs for each aphasic patient. The voxels immediately surrounding the lesion mask (downsampled to a 1 cm resolution) were identified in each participant, and as a control, the same region was defined in the undamaged right hemisphere by reflecting the perilesional mask across the sagittal axis in Talairach space and warping it back to individual space. Areas exhibiting FLAIR hyperintensity were not generally included in the perilesional ROIs, as they were included in the original lesion tracings. Only voxels containing a majority of gray matter were included in the perilesional ROIs, as estimated by automated anatomical segmentation of high-resolution T1 scans, performed in FSL software. This procedure produced ROIs containing structurally intact cortical tissue in all patients, even those with mainly subcortical infarcts.

Relative power and MSE values were then averaged across all included voxels within these ROIs and univariate ANOVAs were conducted to compare the averaged values between groups. Post-hoc comparisons were conducted using Tukey’s HSD test.

The SAM analysis revealed that relative to the young controls, both patients and age-matched controls exhibited increased right hemisphere rolandic beta power compared to younger controls (Fig. 1). To further investigate the signal characteristics in the rolandic region, we extracted averaged power spectra from bilateral rolandic ROIs which consisted of the pre- and post-central gyri as defined by the macroanatomical atlas.

2.6.4. Correlations with activity

To test whether perilesional abnormalities predict task-induced activation of homologous regions in the right hemisphere, we calculated Pearson correlations of intertrial MSE and relative power at the left perilesional ROIs with subsequent task-related activation (8–30 Hz power decrease during sentence listening compared to the intertrial interval) at respective contralateral homologous ROIs.

2.6.5. Single subject maps

One objective of the current study is to present a methodology to identify dysfunctional tissue within each individual patient. Thus, we present two approaches for creating single subject maps.

In one approach, we adopted a methodology used in Muhlau et al. (2009) for voxel-based morphometry of individual patients. Briefly, unequal two-sample t -tests were performed at each voxel comparing an individual patient’s score against the mean of each control group. To calculate the t -score at each voxel, the difference between each patient’s score and each control group’s mean was divided by a pooled variance estimate. This resulted in two t -maps for each patient: one vs. young controls and one vs. age-matched controls. These maps were overlaid on top of the individual structural MRI to identify the dysfunctional perilesional tissue on the individual subject level.

We also present an alternative approach for single subject mapping that does not require data from a control group. Specifically, z -score maps were created by comparing each voxel within an individual’s brain against the mean and standard deviation calculated from all voxels within the brain (including the lesioned area). This approach highlights areas in which brain electrical activity differs strongly from the rest of the brain, and in our experience, does not show patterns of significant alterations within the brains of healthy control subjects.

2.6.6. Correlations between measures

To better understand the general relationship between spectral band power and MSE, as measures of neural activity, we calculated

Pearson's correlations between MSE and relative power at each frequency band and between MSE and the ratio of low (delta + theta) to high (beta) frequency power. In controls, the whole cortex was used as an ROI. We also tested whether the relationship between spectral power and MSE would change as a result of brain pathology, by computing the correlations within the perilesional ROI.

3. Results

3.1.1. Voxel-wise maps – aphasia vs. controls

Fig. 1 presents the comparison maps of relative power and MSE between groups and Table 1 summarizes these results for each hemisphere. Voxels with significant differences are colored and overlaid on an artificially darkened average anatomical image representing the lesion distribution across patients; the darker regions correspond to areas with greater lesion overlap. The highest lesion overlap occurred in the left inferior frontal and superior temporal areas, consistent with typical infarct patterns resulting from left middle cerebral artery occlusion, the most common cause of aphasia (Phan et al., 2005). Fig. 1 presents maps estimated from the baseline intertrial period and from the sentence listening and memory delay period of the task. Visual inspection indicates that the estimates from the two periods revealed very similar patterns of results, with slightly more sensitivity associated with the estimates from the baseline period. As such, the following section will focus on the findings from the baseline period, which represents a better estimation of spontaneous neural activity.

3.1.2. Patients vs. young controls

In the left hemisphere, patients exhibited significantly increased delta and theta power and significantly reduced beta power and MSE posterior to the region of maximal lesion overlap. Patients also exhibited reduced beta power and MSE anterior to the region of maximal lesion overlap.

In the right hemisphere, patients exhibited significantly reduced delta and theta power in the superior temporal, inferior parietal and rolandic regions. Patients also exhibited increased rolandic beta.

3.1.3. Patients vs. age-matched controls

In the left hemisphere, patients exhibited significantly increased delta and theta power and significantly reduced beta power and MSE posterior to the region of maximal lesion overlap. Patients also exhibited reduced beta power and MSE anterior to the region of maximal lesion overlap.

There were no significant differences between patients and age-matched controls in the right hemisphere.

3.1.4. Age-matched vs. young controls

In general, both control groups exhibited similar relative power values across the whole brain. Differences were noted in the delta, theta, and beta bands. Specifically, age-matched controls exhibited decreased left hemisphere delta power in the posterior temporal areas and significantly decreased right hemisphere theta power in the inferior parietal, rolandic and inferior frontal areas, relative to younger controls. Age-matched controls also exhibited bilaterally increased beta power in rolandic regions (precentral and postcentral gyri).

3.2. Task activation

Fig. 2a–c presents the group level activation maps for patients and controls; activation is reflected as the magnitude of a 8–30 Hz power reduction (desynchronization). Young and age matched controls exhibited primarily left lateralized ventral activation. In the patients, left hemisphere activation is localized to the perilesional tissue anterior to

the lesion while right hemisphere activation in the patients was localized to the contralateral homologues of the lesioned and perilesional tissues. These maps are thresholded by activation magnitude (effect size), as the average pseudo-T value across subjects. An arbitrary effect size threshold of 0.5 is used here to avoid differences in the extent of statistically significant activation related to different numbers of subjects in the three groups. The activation magnitude maps are shown here to demonstrate the increased degree of right hemisphere activation in stroke patients, as the region of interest analysis (Section 3.3.5) examined correlations between perilesional dysfunction and compensatory activation of the right hemisphere.

Fig. 2d–f presents statistical maps comparing task-related 8–30 Hz desynchronization between groups. Compared to the young and age-matched controls, the patients exhibited a significant deficit in desynchronization (Fig. 2d–e; reflected by positive t-values) in the temporoparietal junction. Increased right hemisphere activity in patients reached statistical significance relative to the young controls (Fig. 2d) but not compared to the age-matched controls (Fig. 2e). The presence of right-hemisphere activation was highly variable across patients. Therefore, we conducted subsequent ROI-based correlation analyses to assess possible associations between the degree of left-hemisphere perilesional dysfunction and right-hemisphere task activation (Section 3.3.5). The age-matched controls exhibited increased left hemisphere rolandic desynchronization relative to young controls.

3.3. Region of interest analyses

3.3.1. Atlas-based anterior ROI

Fig. 3a–b presents the power spectra extracted from the four atlas-based ROIs. In the left hemisphere anterior ROI, there was a significant main effect of group for relative beta power, $F(2,55) = 5.840$, $p < 0.01$. Post-hoc analyses using Tukey's HSD test revealed that beta power was significantly lower in patients ($M = 0.185$, $SEM = 0.011$) when compared to the young ($M = 0.218$, $SEM = 0.011$) and age-matched controls ($M = 0.253$, $SEM = 0.018$). The main effects of relative delta, $F(2,55) = 1.767$, $p = 0.181$, theta, $F(2,55) = 2.409$, $p = 0.099$ and alpha, $F(2,55) = 0.538$, $p = 0.587$, were not significant.

There was also a main effect of MSE, $F(2,55) = 6.240$, $p < 0.01$; MSE was significantly lower in patients ($M = 1.784$, $SEM = 0.012$) when compared to the young ($M = 1.837$, $SEM = 0.013$) and age-matched controls ($M = 1.852$, $SEM = 0.021$).

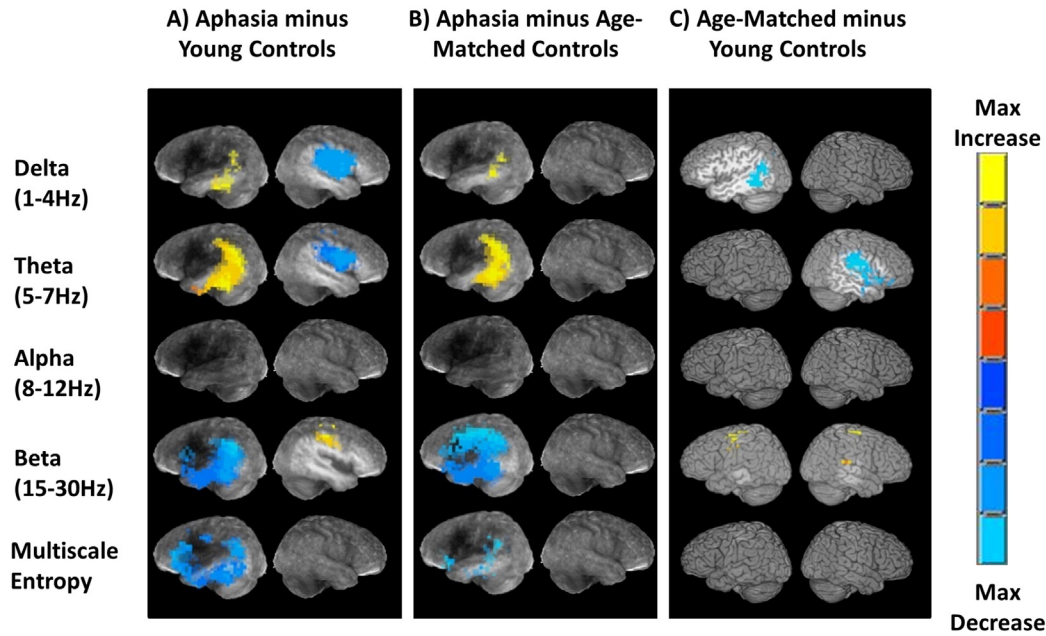
In the right hemisphere, there were no significant main effects of relative delta, $F(2,55) = 1.711$, $p = 0.190$, relative theta, $F(2,55) = 2.006$, $p = 0.144$, relative alpha, $F(2,55) = 0.171$, $p = 0.844$, relative beta, $F(2,55) = 1.643$, $p = 0.203$, or MSE, $F(2,55) = 0.730$, $p = 0.487$.

3.3.2. Atlas-based posterior ROI

In the left hemisphere posterior ROI, there were significant main effects of relative power in the delta, $F(2,55) = 5.992$, $p < 0.01$, theta, $F(2,55) = 12.331$, $p < 0.001$ and beta, $F(2,55) = 10.106$, $p < 0.001$, frequency bands. Post-hoc analyses revealed that delta power was significantly higher in patients ($M = 0.110$, $SEM = 0.001$) when compared to the young ($M = 0.090$, $SEM = 0.001$) and age-matched controls ($M = 0.073$, $SEM = 0.011$). Theta band power was also significantly higher in patients ($M = 0.115$, $SEM = 0.005$) when compared to young ($M = 0.090$, $SEM = 0.005$) and age-matched controls ($M = 0.076$, $SEM = 0.008$). The patients also exhibited significantly reduced relative beta power ($M = 0.160$, $SD = 0.010$) when compared to the young ($M = 0.210$, $SD = 0.010$) and age-matched controls ($M = 0.237$, $SD = 0.017$). There were no significant group differences in relative alpha power, $F(2,55) = 0.544$, $p = 0.446$.

There was also a significant main effect of MSE, $F(2,55) = 9.636$, $p < 0.001$. Patients exhibited significantly decreased MSE ($M = 1.755$, $SEM = 0.011$) when compared to the young ($M = 1.843$, $SEM = 0.011$) and age-matched controls ($M = 1.821$, $SEM = 0.017$).

Baseline



Sentence Listening

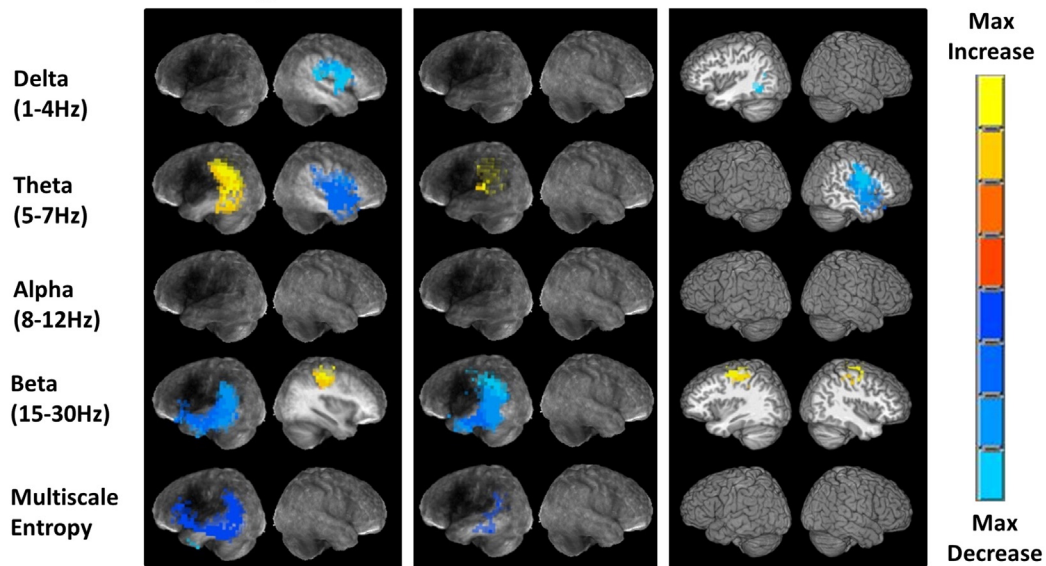


Fig. 1. Voxel-wise contrasts from baseline (upper) and sentence listening (lower) periods of the task. T-test maps of relative power and MSE overlaid on top of an artificially darkened render representing the lesion distribution across patients; darker regions correspond to areas with greater lesion overlap. The maps contrast patients minus young controls (A), patients minus age-matched controls (B), and age-matched controls minus young controls (C). Active voxels are color coded according to the magnitude of difference and thresholded at $p < 0.05$, corrected.

In the right hemisphere ROI, there was a marginally significant main effect of group for relative delta power, $F(2,55) = 2.796$, $p = 0.069$. However, post-hoc analyses with Tukey’s HSD test revealed no

differences between the patients ($M = 0.078$, $SEM = 0.005$), and the young ($M = 0.092$, $SD = 0.005$) and age-matched controls ($M = 0.076$, $SEM = 0.008$). There were no main effects of group in the

Table 1
Summary of the results from the SAM analysis of spontaneous activity within each hemisphere. ‘Increased’ indicates the contrast yielded at least one significant cluster of positive voxels ($p < 0.05$, corrected), ‘decreased’ indicates the opposite; Ns. = no significant clusters.

	Patients minus young controls		Patients minus age-matched controls		Age-matched minus young controls	
	Left hemisphere	Right hemisphere	Left hemisphere	Right hemisphere	Left hemisphere	Right hemisphere
Delta (1–4 Hz)	Increased	Decreased	Increased	Ns.	Decreased	Ns.
Theta (5–7 Hz)	Increased	Decreased	Increased	Ns.	Ns.	Decreased
Alpha (8–12 Hz)	Ns.	Ns.	Ns.	Ns.	Ns.	Ns.
Beta (15–30 Hz)	Decreased	Increased	Decreased	Ns.	Increased	Increased
MSE	Decreased	Ns.	Decreased	Ns.	Ns.	Ns.

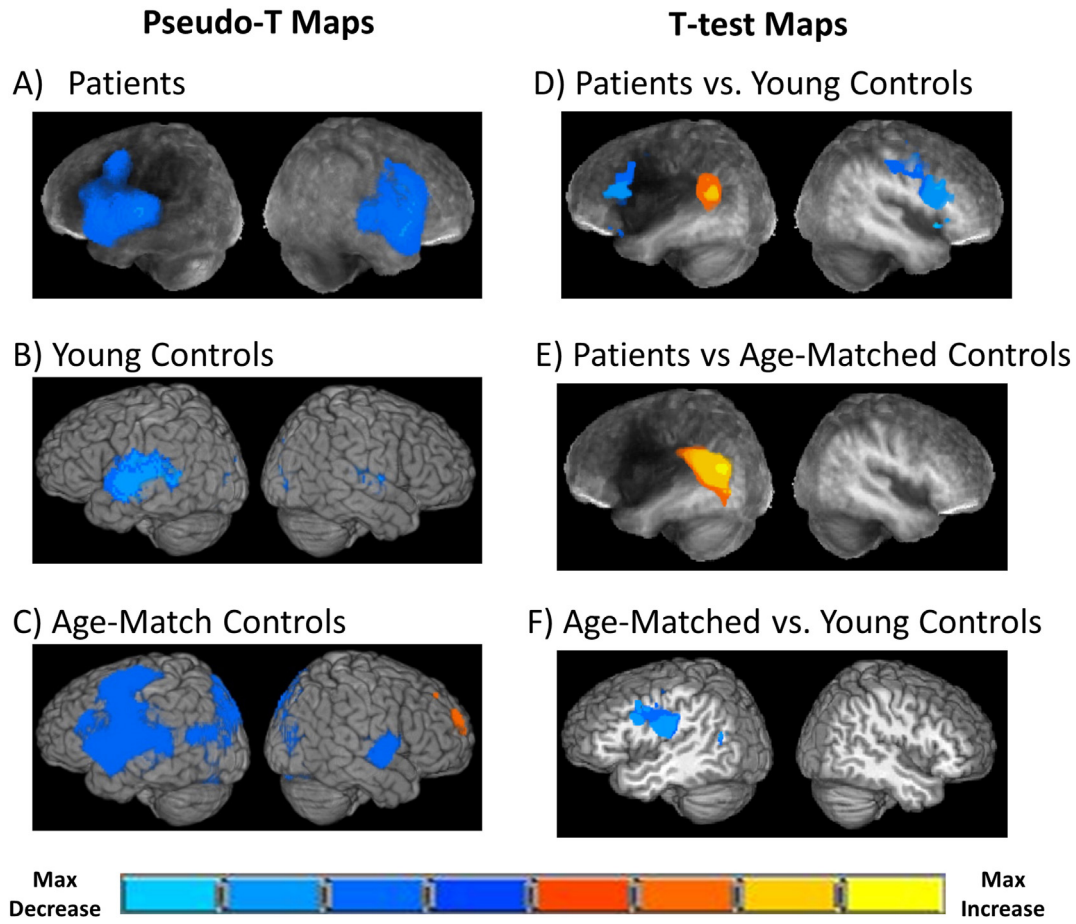


Fig. 2. Task activation maps. Pseudo-T maps (left panel) presenting an 8–30 Hz event related desynchronization during the sentence listening period of the task for patients (A), young controls (B) and age-matched controls (C). These maps represent the average magnitude of activation across subjects (effect size), and are thresholded at an arbitrary level of 0.5, to avoid differences related to different numbers of subjects in the groups. T-test maps (right panel) contrast patients minus young controls (D), patients minus age-matched controls, and (F), age-matched minus young controls. Active voxels are color coded according to the magnitude of difference and thresholded at $p < 0.05$, corrected.

theta, $F(2,55) = 2.338$, $p = 0.106$, alpha, $F(2,55) = 0.310$, $p = 0.310$ and beta, $F(2,55) = 2.113$, $p = 0.131$, frequency bands. The main effect of MSE was also not significant, $F(2,55) = 0.100$, $p = 0.905$.

3.3.3. Perilesional ROI

Fig. 3d presents the locations of a perilesional ROI and its contralesional mirror ROI in one sample subject, along with the power spectra averaged across subjects from the two ROIs. Note that the ROI does not appear perfectly symmetrical in both hemispheres due to the distortion of the left hemisphere structures by the lesion. Paired t-tests revealed that the perilesional ROI exhibited significantly increased delta, $t(24) = 5.15$, $p < 0.001$, and theta power $t(24) = 7.051$, $p < 0.001$ as well as significantly reduced beta power, $t(24) = 11.475$, $p < 0.001$, compared to the contralesional ROI. The difference in relative alpha power was not significant, $t(24) = 1.464$, $p = 0.156$.

The left hemisphere perilesional ROI also exhibited significantly reduced MSE, $t(24) = 6.578$, $p < 0.001$, when compared to the contralateral mirror ROI.

3.3.4. Rolandic ROI

Fig. 3e presents the average power spectra from the bilateral rolandic ROIs for all groups. Across both hemispheres, differences between spectra are most notable along the beta band. Specifically, right hemisphere beta power is increased for the patients and age-matched controls, while left hemisphere beta is increased only for the age-matched controls.

3.3.5. Correlations with homologue task activation

Fig. 4 presents scatterplots of right hemisphere homologue task activation as a function of intertrial MSE and relative power in left hemisphere perilesional areas. Perilesional relative delta power was positively associated with right hemisphere homologue task activation ($r(23) = 0.516$, $p < 0.01$), while perilesional MSE was negatively associated with right hemisphere homologue activation ($r(23) = -0.540$, $p < 0.01$). There were no significant correlations between right hemisphere task activation and perilesional relative theta ($r(23) = 0.321$, $p > 0.118$), relative alpha ($r(23) = -0.164$, $p = 0.433$), and relative beta ($r(23) = -0.271$, $p = 0.191$).

3.4. Single subject mapping

Thresholded single subject maps of relative theta power and MSE are shown in Fig. 5 for one patient with a perisylvian lesion and one patient with a subcortical lesion. For both patients, MSE was reduced and theta was increased. The magnitude and spatial extent of perilesional dysfunction as detected by the t-score and z-score methods were comparable. To illustrate the sensitivity of the different measures for single subject mapping and to estimate the incidence of detectable abnormalities in perilesional tissue in individual patients, we calculated the proportion of voxels that exhibited significant t-scores vs. age-matched controls ($p < 0.05$, uncorrected), within each individual's perilesional ROI (Fig. 6).

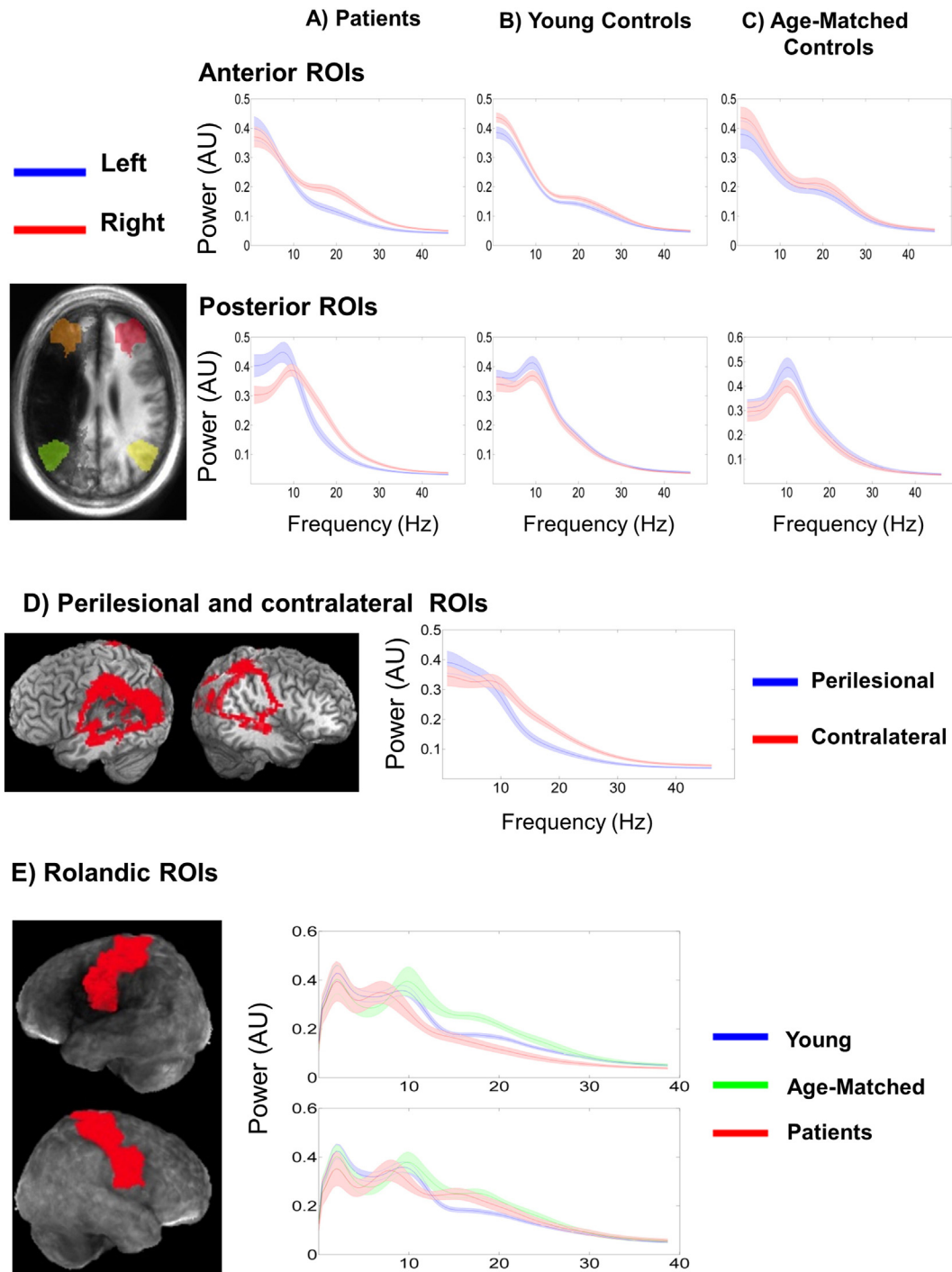


Fig. 3. Power spectra averaged across all voxels from the atlas-based (top), perilesional and contralateral (middle), and rolandic (bottom) ROIs. Spectra from homologous ROIs are plotted together: left hemisphere in blue and right hemisphere in red. Spectra are plotted separately for patients (A), young controls (B), and age-matched controls (C). Spectra from the perilesional and contralateral ROIs, averaged across all subjects, are plotted together (D): left hemisphere in blue and right hemisphere in red. The displayed lesion and perilesional ROIs are from the single sample subject. (E) Averaged spectra from the three groups are plotted together for the left (top) and right (bottom) rolandic ROIs. Shaded regions represent the standard error of the mean power estimate.

3.5. Correlations between MSE and spectral band power

Table 2 presents correlations of MSE and relative band power across the entire cortex for controls and in the perilesional areas of patients. In the young controls there were significant negative correlations between MSE and relative delta, $r(22) = -0.638$, $p < 0.01$, relative theta, $r(22) = -0.702$, $p < 0.01$, and the (delta + theta)/beta ratio, $r(22) = -0.828$, $p < 0.01$. MSE also positively correlated with relative beta power, $r(22) = 0.815$, $p < 0.01$. MSE did not correlate with relative

alpha power, $r(22) = 0.043$, $p = 0.849$. As demonstrated in Table 1, the same pattern of correlations between MSE and spectral power was also present in the age-matched controls and in the perilesional tissue.

4. Discussion

This study illustrates a novel approach to the characterization of altered spontaneous electrical activity generated by perilesional areas following stroke. Building on previous EEG and MEG studies, both spectral

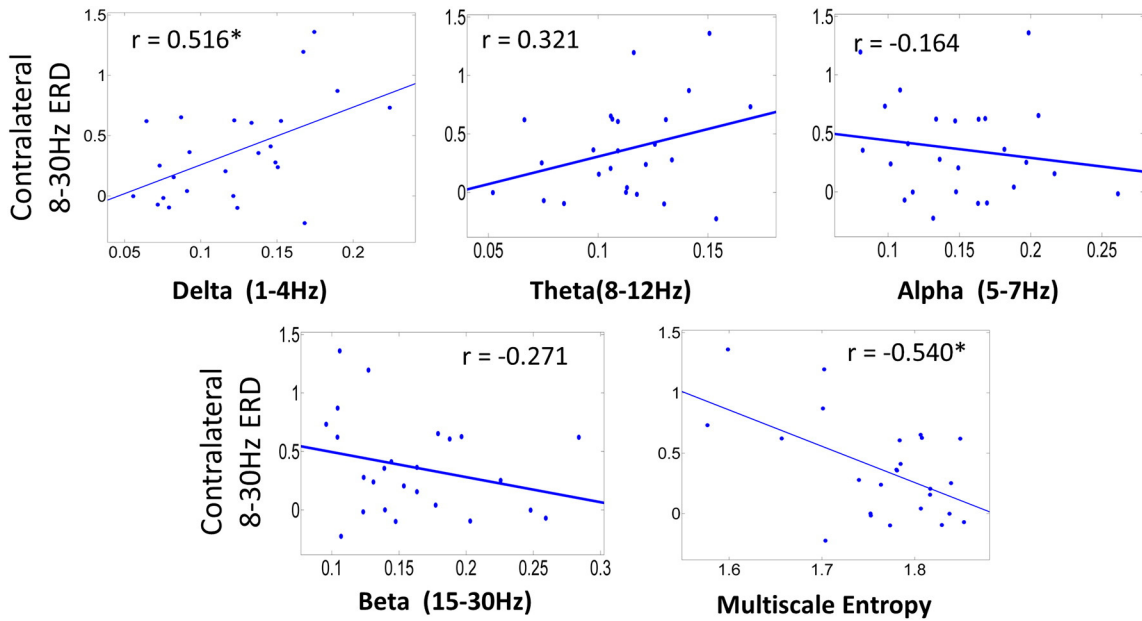


Fig. 4. The magnitude of contralateral homologous task activation (8–30 Hz ERD) plotted as a function of perilesional relative delta, theta, alpha, beta, and MSE (B). Pearson’s correlations are presented with each figure. *Significant at $p < 0.05$.

and nonlinear analyses of electrophysiological data revealed robust group differences between patients with stroke and healthy controls, and between the affected and unaffected hemispheres (e.g., Finnigan et al., 2004; Finnigan and van Putten, 2013; Tecchio et al., 2006, 2005). Whereas previous studies of spontaneous electrical activity in stroke have largely focused on increased low frequency signals, the present

study presents a method for source analysis of low amplitude high frequency activity, and characterization of signals using nonlinear algorithms in source space.

The analysis of different signal measures in a common source space allowed us to evaluate differences in sensitivity between them. For example, SAM maps of reduced MSE and relative beta in patients vs.

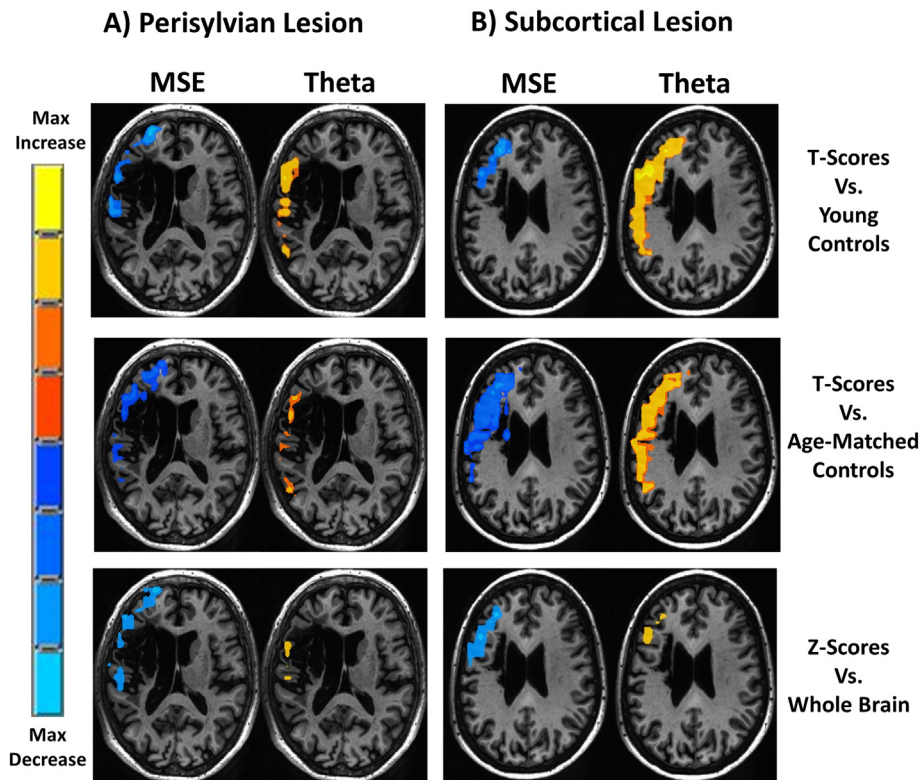


Fig. 5. Single subject maps. Maps of baseline relative theta (right) and MSE (left) are presented for a patient with a left hemisphere perisylvian lesion (A) and a patient with an anterior subcortical lesion (B). T-score maps were computed by comparing the single subject’s value at each voxel vs. the mean and standard deviation of the young (upper) and age-matched (middle) control groups. Z-score maps (lower) were computed by comparing each voxel vs. the mean and standard deviation of all voxels in the individual’s brain. Active voxels are color coded according to the magnitude of difference and thresholded at $p < 0.05$, uncorrected.

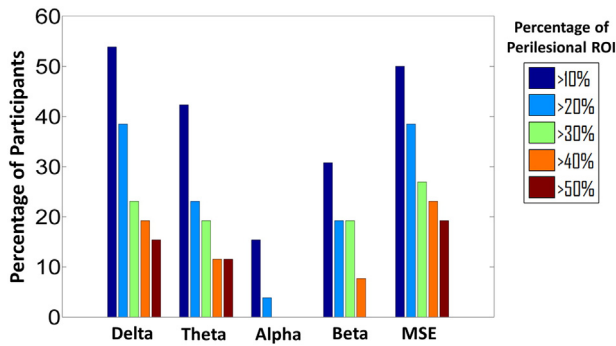


Fig. 6. Bar graph illustrating the proportion of participants with significant perilesional changes in relative power and MSE compared to the age-matched controls (significant single subject *t*-scores; $p < 0.05$, uncorrected). The colored bars represent different proportions of the perilesional ROI with significant voxels.

controls revealed significant voxels in areas anterior and posterior to the areas of maximal lesion overlap, while maps of increased relative theta and delta revealed significant voxels only posterior to the lesion zone. This is further confirmed by ROI analyses demonstrating that MSE, delta, theta, and beta measures were sensitive to changes in the posterior ROI, while only MSE and beta power were sensitive to dysfunction in the anterior ROI. This particular distinction between the anterior and posterior regions most likely reflects the idiosyncratic nature of the present sample of patients, whose lesions were distributed in various areas centered on the left perisylvian cortex. However, these results suggest that reductions in MSE and beta power may be equally or even more sensitive than the more commonly used measures of low-frequency power increase.

Some limitations apply for this study, and suggest directions for future research. One limitation is that true “resting” MEG data were not available in these patients. Patients were originally recruited for an MEG study of language processing, and the timing of the procedures was optimized to maximize sensitivity for that study. In the present re-analysis of that MEG data, we examined “spontaneous” data from the intertrial interval of the language task. Similar results were obtained from data in the task periods. Thus, there is some concern that the brief intertrial intervals included task-related neural activity ‘spilled over’ from the previous trial. However, given that neural activity results in a decrease in 8–30 Hz power (Brookes et al., 2005; Hillebrand et al., 2005; Singh et al., 2002), such spillover would result in reduced 8–30 Hz power for active tissue relative to inactive tissue. Our results demonstrated the opposite: perilesional tissue exhibited reduced beta-band power (15–30 Hz) relative to healthy tissue from both control groups.

Nonetheless, true resting data would be desirable. Based on the present findings, we now consider it worthwhile to routinely collect at least 5 min of resting data from stroke patients participating in MEG studies. Studies underway in our laboratory are also assessing correlations between perilesional MEG abnormalities and MRI-based measures such as white matter integrity (assessed with FLAIR and diffusion tensor imaging) and blood flow (assessed with arterial spin labeling). These

Table 2

Correlations of MSE and relative power. Correlations were computed across subjects, between MSE and relative delta, theta, alpha & beta averaged across the whole cortex for controls and across perilesional tissue for patients.

	Young controls	Age-matched controls	Patients
Delta	−0.638**	−0.785*	−0.856**
Theta	−0.702**	−0.757*	−0.855**
Alpha	0.043	−0.285	0.222
Beta	0.815**	0.844**	0.810**
Delta–theta/beta ratio	−0.828**	−0.851**	−0.938**

* $p < 0.05$.

** $p < 0.01$.

studies have the potential to reveal the underlying mechanisms that may contribute to tissue dysfunction, such as white matter disconnection and hypoperfusion.

Another limitation of the present study is the difficulty in conducting group statistical analysis in a heterogeneous sample of patients. The patients did have some commonalities: all had a single left-hemisphere stroke impinging on perisylvian language regions, leading to aphasia but there was also considerable variability in aphasia symptoms, and lesion location and extent. We dealt with this heterogeneity by conducting several complementary analyses, based on whole-brain mapping, consistent atlas-based ROIs, and customized perilesional ROIs. Each had drawbacks: the whole-brain mapping ignores the lesion location, the atlas-based ROIs are perilesional in some subjects but not others, and the customized perilesional ROIs have widely variable size and location across participants. Fortunately all analyses converged on the same conclusions: perilesional tissue consistently exhibited reduced high frequency activity and MSE, and in some regions also showed increased low frequency activity. In fact, we anticipate that the methods presented in this paper will ultimately be more useful for analysis of individual patients in a clinical/therapeutic context (see Section 4.3), obviating the problems associated with group analysis.

Together, the findings support the utility of both spectral and nonlinear time series measures in source space to identify neural dysfunction in the perilesional tissue, and suggest that identification of increased delta-range activity alone may provide an incomplete characterization of altered spontaneous neural dynamics after stroke.

4.1. Relationship between spectral and nonlinear measures

While there were differences between maps based on spectral measures and multi-scale entropy, they were overall quite similar, raising the question of whether these techniques provide complementary information, or instead represent two ways of quantifying essentially the same phenomenon. Besides the visual comparison of statistical maps generated from both techniques, we also assessed direct correlations between MSE and spectral power across subjects in patients and controls, testing whether there was a close association between these measures in normal, healthy tissue. In all groups, MSE was positively correlated with beta power, but negatively with delta and theta power, and not significantly correlated with alpha power. Thus, MSE seems to closely covary with the ratio of higher frequencies to lower frequencies in an electrophysiological signal, at least at the time scales that we assessed. This intuition was confirmed by directly assessing the correlation between MSE and the (delta + theta)/beta power ratio, which was stronger than the correlation with any individual frequency band. A similar conclusion was reached by Bruce et al. (2009) who compared SampEn and spectral measures in EEG obtained from adults during wakefulness and sleep, and also obtained similar results from simulated EEG signals.

One difference noted between the spectral measures and MSE related to the effects of aging deserves some special scrutiny. We did not observe any differences in MSE between the younger controls and the age-matched controls (Fig. 1c). However, age-matched controls exhibited bilateral increased relative beta power, and decreased delta/theta power, which seemed to be a general effect of aging rather than an indication of disease-related pathology. This general speeding of the signal is also present in the unaffected right hemisphere of the patients, when compared to the young controls. Furthermore the power spectra from the right rolandic ROI (Fig. 3e) clearly shows increased beta power for both patients and age-matched controls.

This finding is in line with previous reports of age-related speeding of electrical activity. Bruce et al. (2009) found decreased relative delta and increased relative beta associated with aging during wakefulness and sleep. Feinberg and Campbell (2003) also found reduced delta associated with aging during sleep, while Mann and Roschke (2004) found a significant negative correlation between age and delta/theta power

measured during sleep. This speeding of the frequency spectrum may seem contrary to behavioral and electrophysiological studies demonstrating age-related increases in the latency of response time and ERPs (Rossini et al., 2007). However, Hong and Rebec (2012) proposed that the speeding of the frequency spectrum may actually reflect compensatory speeding of firing rates. Specifically, the authors suggest that aging associated increases in conduction delays will progressively increase the phase difference between synchronized neurons until they are in antiphase. To compensate, one neuron must double the firing rate to realign their excitability peaks. This compensatory speeding will be reflected as a shift of the frequency spectrum from low to high frequencies. It should be noted that the authors hypothesized aging related increases in gamma power while we observed increased beta. This is likely due to the fact that the speeding was observed in the rolandic regions where idle beta activity is dominant (Ritter et al., 2009). Our findings are consistent with a previous report of increased relative and absolute beta power in older adults compared to younger adults (Holschneider and Leuchter, 1995).

Notably, the MSE measures were not significantly affected by this increase in relative beta power present in older participants. Therefore, it is possible that MSE could provide a more specific indicator of perilesional dysfunction in stroke, dissociable from the effects of aging. Future studies including larger groups of participants at various age levels are needed to fully dissociate the role of aging in altered neural dynamics commonly seen in patients with neurological disorders.

4.2. Compensatory right hemisphere activation

The activation maps presented here converge with a multitude of studies demonstrating right hemisphere language activation in chronic aphasia (Musso et al., 1999; Thulborn et al., 1999; Tillema et al., 2008). Specifically, we found a bilateral pattern of activation in aphasic patients during language processing, while the younger and older controls exhibited strong left-lateralization. Despite the bilateral pattern seen in the patients, increased right-hemisphere activation in the patients as a group was not statistically significant compared to the age-matched controls (Fig. 2e). This may be due to the low power resulting from a smaller group of older controls, but is also related to the high degree of variability across the patient group in lesion characteristics and right-hemisphere activation. In our previous study with this cohort, we characterized the relationship between language comprehension performance and differential activation to sentences of varying difficulty levels, finding a correlation between right hemisphere activation and successful comprehension (Meltzer et al., 2013). However, in that study, positive correlations with performance were not generally in homologous regions to those associated with comprehension performance based on lesion analysis; this suggests that compensatory activity may reflect adaptive recruitment of alternative strategies rather than homologous takeover of the same cognitive functions.

In the present study, we examined a simpler contrast of sentence listening vs. the prestimulus baseline, to test whether there was any association between the degree of right hemisphere activation present in each patient and the degree of perilesional dysfunction detected during the intertrial period. We did find such an association: perilesional dysfunction (increased slowing and reduced entropy) was correlated with task activation in the right hemisphere homologue of the perilesional tissue. Thus, the current results provide evidence for homologous takeover during basic sentence processing, which is modulated by the magnitude of the left hemisphere dysfunction. Some authors have suggested that the activation of right hemisphere homologues of the language areas may reflect a release of transcallosal inhibition from the damaged left hemisphere (Martin et al., 2004; Thiel et al., 2006b). The current findings are consistent with this hypothesis, but do not test this hypothesis directly. We are currently exploring effective connectivity analyses to directly test the hypothesis of transcallosal inhibition in stroke.

4.3. Identifying targets for non-invasive stimulation-based intervention

The role of right hemisphere activation in residual language processing is still debated though evidence suggests that the best outcome is associated with a reintegration of the surviving perilesional regions into the language network (Saur et al., 2006). Therapeutic studies of noninvasive brain stimulation typically aim to increase the activation of structurally intact perilesional cortex, either by direct excitatory stimulation of that tissue (Marangolo et al., 2013; Szaflarski et al., 2011), or by inhibitory stimulation to the contralateral hemisphere (Abo et al., 2012; Barwood et al., 2011, 2013; Kakuda et al., 2011; Kindler et al., 2012; Naeser et al., 2005b; Medina et al., 2012; Naeser et al., 2010; Thiel et al., 2013, 2006a; Waldowski et al., 2012; Weiduschat et al., 2011; Winhuisen et al., 2007). However, there is also evidence of beneficial outcomes associated with excitatory right hemisphere stimulation (Flöel et al., 2011). It is likely that a multitude of factors contribute to the overall relationship between stimulation site and behavioral outcome, including lesion size, location, pre-stroke laterality and structural and functional integrity of the perilesional tissue.

The methods demonstrated here provide a means to identify dysfunctional perilesional tissue potentially suitable for physiological interventions such as transcranial magnetic stimulation (TMS) and transcranial direct current stimulation (tDCS). The fact that stimulation of the perilesional cortex can improve behavioral outcomes suggests that the dysfunctional perilesional tissue has the capacity for successful reintegration into the language network. Critically, such regions may be ideal targets for intervention as numerous studies have demonstrated that the best clinical outcome in aphasia is associated with reactivation of the perilesional tissue. The single subject mapping approaches presented here provide a means to identify tissue within an individual patient that is most likely to benefit from non-invasive stimulation, and could also allow researchers to assess both short-term and long-term changes in cortical activity induced by the stimulation. It should be noted that the single subject maps from some patients did not show perilesional dysfunction. As such, it stands to reason that these patients may not benefit from direct perilesional stimulation. The clinical utility of the single subject maps lies in its ability to identify ideal candidate patients and brain regions for stimulation-based rehabilitation. Thus, mapping of perilesional dysfunction is likely to play an important role in the future development of physiologically informed neurorehabilitation programs in stroke.

Acknowledgments

We thank the participating patients and their families. Data collection was funded by the Intramural Research Program of the National Institute on Deafness and Other Communication Disorders. Later analyses were supported by grants from the Heart and Stroke Foundation Canadian Partnership for Stroke Recovery and the Alzheimer's Association.

References

- Abo, M., Kakuda, W., Watanabe, M., Morooka, A., Kawakami, K., Senoo, A., 2012. Effectiveness of low-frequency rTMS and intensive speech therapy in poststroke patients with aphasia: a pilot study based on evaluation by fMRI in relation to type of aphasia. *Eur. Neurol.* 68 (4), 199–208. <http://dx.doi.org/10.1159/00033877322948550>.
- Barwood, C.H., Murdoch, B.E., Riek, S., O'Sullivan, J.D., Wong, A., Lloyd, D., Coulthard, A., 2013. Long term language recovery subsequent to low frequency rTMS in chronic non-fluent aphasia. *NeuroRehabilitation* 32 (4), 915–928. <http://dx.doi.org/10.3233/NRE-13091523867417>.
- Barwood, C.H., Murdoch, B.E., Whelan, B.M., Lloyd, D., Riek, S., O' Sullivan, J.D., Coulthard, A., Wong, A., 2011. Improved language performance subsequent to low-frequency rTMS in patients with chronic non-fluent aphasia post-stroke. *Eur. J. Neurol.* 18 (7), 935–943. <http://dx.doi.org/10.1111/j.1468-1331.2010.03284.x21138505>.
- Bosl, W., Tierney, A., Tager-Flusberg, H., Nelson, C., 2011. EEG complexity as a biomarker for autism spectrum disorder risk. *B.M.C. Med.* 9, 18. <http://dx.doi.org/10.1186/1741-7015-9-1821342500>.
- Brookes, M.J., Gibson, A.M., Hall, S.D., Furlong, P.L., Barnes, G.R., Hillebrand, A., Singh, K.D., Holliday, I.E., Francis, S.T., Morris, P.G., 2005. GLM-beamformer method demonstrates stationary field, alpha ERD and gamma ERS co-localisation with fMRI BOLD response

- in visual cortex. *Neuroimage* 26 (1), 302–308. <http://dx.doi.org/10.1016/j.neuroimage.2005.01.05015862231>.
- Bruce, E.N., Bruce, M.C., Venelaganti, S., 2009. Sample entropy tracks changes in electroencephalogram power spectrum with sleep state and aging. *J. Clin. Neurophysiol.* 26 (4), 257–266. <http://dx.doi.org/10.1097/WNP.0b013e3181b2f1e319590434>.
- Butz, M., Gross, J., Timmermann, L., Moll, M., Freund, H.-J., Witte, O.W., Schnitzler, A., 2004. Perilesional pathological oscillatory activity in the magnetoencephalogram of patients with cortical brain lesions. *Neurosci. Lett.* 355 (1–2), 93–96. <http://dx.doi.org/10.1016/j.neulet.2003.10.06514729243>.
- Catarino, A., Churches, O., Baron-Cohen, S., Andrade, A., Ring, H., 2011. Atypical EEG complexity in autism spectrum conditions: a multiscale entropy analysis. *Clin. Neurophysiol.* 122 (12), 2375–2383. <http://dx.doi.org/10.1016/j.clinph.2011.05.00421641861>.
- Cornelissen, K., Laine, M., Tarkiainen, A., Järvensivu, T., Martin, N., Salmelin, R., 2003. Adult brain plasticity elicited by anomia treatment. *J. Cogn. Neurosci.* 15 (3), 444–461. <http://dx.doi.org/10.1162/089989290332159315312729495>.
- Costa, M., Goldberger, A.L., Peng, C.K., 2002. Multiscale entropy analysis of complex physiological time series. *Phys. Rev. Lett.* 89 (6), 068102. <http://dx.doi.org/10.1103/PhysRevLett.89.06810212190613>.
- Costa, M., Goldberger, A.L., Peng, C.K., 2005. Multiscale entropy analysis of biological signals. *Phys Rev E Stat Nonlin Soft Matter Phys* 71 (2 1), 02190615783351.
- Crinion, J., Price, C.J., 2005. Right anterior superior temporal activation predicts auditory sentence comprehension following aphasic stroke. *Brain* 128 (12), 2858–2871. <http://dx.doi.org/10.1093/brain/awh65916234297>.
- Cuspidada, E.R., Machado, C., Virues, T., Martínez-Montes, E., Ojeda, A., Valdés, P.A., Bosch, J., Valdes, L., 2009. Source analysis of alpha rhythm reactivity using LORETA imaging with 64-channel EEG and individual MRI. *Clin. E.E.G. Neurosci.* 40 (3), 150–156. <http://dx.doi.org/10.1177/1550059409040030619715176>.
- Eickhoff, S.B., Stephan, K.E., Mohlberg, H., Grefkes, C., Fink, G.R., Amunts, K., Zilles, K., 2005. A new SPM toolbox for combining probabilistic cytoarchitectonic maps and functional imaging data. *Neuroimage* 25 (4), 1325–1335. <http://dx.doi.org/10.1016/j.neuroimage.2004.12.03415850749>.
- Feinberg, I., Campbell, I.G., 2003. Kinetics of non-rapid eye movement delta production across sleep and waking in young and elderly normal subjects: theoretical implications. *Sleep* 26 (2), 192–200. <http://dx.doi.org/10.1093/sleep/26.2.192>.
- Finnigan, S., van Putten, M.J., 2013. EEG in ischaemic stroke: quantitative EEG can uniquely inform (sub-)acute prognoses and clinical management. *Clin. Neurophysiol.* 124 (1), 10–19. <http://dx.doi.org/10.1016/j.clinph.2012.07.00322858178>.
- Finnigan, S.P., Rose, S.E., Walsh, M., Griffin, M., Janke, A.L., McMahon, K.L., Gillies, R., Strudwick, M.W., Pettigrew, C.M., Semple, J., Brown, J., Brown, P., Chalk, J.B., 2004. Correlation of quantitative EEG in acute ischemic stroke with 30-day NIHSS score: comparison with diffusion and perfusion MRI. *Stroke* 35 (4), 899–903. <http://dx.doi.org/10.1161/01.STR.0000122622.73916.d215001786>.
- Flöel, A., Meinzer, M., Kirstein, R., Nijhof, S., Deppe, M., Knecht, S., Breitenstein, C., 2011. Short-term anomia training and electrical brain stimulation. *Stroke* 42 (7), 2065–2067. <http://dx.doi.org/10.1161/STROKEAHA.110.60903221636820>.
- Harmony, T., Fernández-Bouzas, A., Marosi, E., Fernández, T., Valdés, P., Bosch, J., Riera, J., Bernal, J., Rodríguez, M., Reyes, A., 1995. Frequency source analysis in patients with brain lesions. *Brain Topogr.* 8 (2), 109–117. <http://dx.doi.org/10.1007/BF011997748793121>.
- Heiss, W.-D., Thiel, A., 2006. A proposed regional hierarchy in recovery of post-stroke aphasia. *Brain Lang.* 98 (1), 118–123. <http://dx.doi.org/10.1016/j.bandl.2006.02.00216564566>.
- Hillebrand, A., Singh, K.D., Holliday, I.E., Furlong, P.L., Barnes, G.R., 2005. A new approach to neuroimaging with magnetoencephalography. *Hum. Brain Mapp.* 25 (2), 199–211. <http://dx.doi.org/10.1002/hbm.2010215846771>.
- Hofmeijer, J., van Putten, M.J., 2012. Ischemic cerebral damage: an appraisal of synaptic failure. *Stroke* 43 (2), 607–615. <http://dx.doi.org/10.1161/STROKEAHA.111.63294322207505>.
- Holschneider, D.P., Leuchter, A.F., 1995. Beta activity in aging and dementia. *Brain Topogr.* 8 (2), 169–180.
- Hong, S.L., Rebec, G.V., 2012. A new perspective on behavioral inconsistency and neural noise in aging: compensatory speeding of neural communication. *Front. Aging Neurosci.* 4, 27. <http://dx.doi.org/10.3389/fnagi.2012.0002723055970>.
- Hornero, R., Escudero, J., Fernández, A., Poza, J., Gómez, C., 2008. Spectral and nonlinear analyses of MEG background activity in patients with Alzheimer's disease. *I. E.E.E. Trans. Biomed. Eng.* 55 (6), 1658–1665. <http://dx.doi.org/10.1109/TBME.2008.91987218714829>.
- Kakuda, W., Abo, M., Momosaki, R., Morooka, A., 2011. Therapeutic application of 6-Hz primed low-frequency rTMS combined with intensive speech therapy for post-stroke aphasia. *Brain Inj* 25 (12), 1242–1248. <http://dx.doi.org/10.3109/02699052.2011.60821221902549>.
- Kang, E.K., Kim, Y.K., Sohn, H.M., Cohen, L.G., Paik, N.J., 2011. Improved picture naming in aphasia patients treated with cathodal tDCS to inhibit the right Broca's homologue area. *Restor. Neurol. Neurosci.* 29 (3), 141–152. <http://dx.doi.org/10.3233/RNN-2011-058721586821>.
- Kindler, J., Schumacher, R., Cazzoli, D., Gutbrod, K., Koenig, M., Nyffeler, T., Dierks, T., Müri, R.M., 2012. Theta burst stimulation over the right Broca's homologue induces improvement of naming in aphasic patients. *Stroke* 43 (8), 2175–2179. <http://dx.doi.org/10.1161/STROKEAHA.111.647503>.
- Lake, D.E., Richman, J.S., Griffin, M.P., Moorman, J.R., 2002. Sample entropy analysis of neonatal heart rate variability. *Am. J. Physiol. Heart Circ. Physiol.* 283 (3), R789–R797. <http://dx.doi.org/10.1152/ajpregu.00069.2002>.
- Luckhoo, H.T., Brookes, M.J., Woolrich, M.W., 2014. Multi-session statistics on beamformed MEG data. *Neuroimage* 95, 330–335. <http://dx.doi.org/10.1016/j.neuroimage.2013.12.02624412400>.
- Machado, C., Cuspidada, E., Valdés, P., Virues, T., Llopis, F., Bosch, J., Aubert, E., Hernández, E., Pando, A., Alvarez, M.A., Barroso, E., Galán, L., Avila, Y., 2004. Assessing acute middle cerebral artery ischemic stroke by quantitative electric tomography. *Clin. E.E.G. Neurosci.* 35 (3), 116–124. <http://dx.doi.org/10.1162/089989290332159315312729495>.
- Mann, K., Röschke, J., 2004. Influence of age on the interrelation between EEG frequency bands during NREM and REM sleep. *Int. J. Neurosci.* 114 (4), 559–571. <http://dx.doi.org/10.1080/0020745049042270415195358>.
- Marangolo, P., Fiori, V., Calpagnano, M.A., Campana, S., Razzano, C., Caltagirone, C., Marini, A., 2013. tDCS over the left inferior frontal cortex improves speech production in aphasia. *Front. Hum. Neurosci.* 7, 539. <http://dx.doi.org/10.3389/fnhum.2013.0053924046740>.
- Martin, P.I., Naeser, M.A., Theoret, H., Tormos, J.M., Nicholas, M., Kurland, J., Fregni, F., Seekins, H., Doron, K., Pascual-Leone, A., 2004. Transcranial magnetic stimulation as a complementary treatment for aphasia. *Semin. Speech Lang.* 25 (2), 181–191. <http://dx.doi.org/10.1055/s-2004-82565415118944>.
- McCubbin, J., Vrba, J., Spear, P., McKenzie, D., Willis, R., Loewen, R., Robinson, S.E., Fife, A.A., 2004. Advanced electronics for the CTF MEG system. *Neurol. Clin. Neurophysiol.* 2004, 6916012695.
- Medina, J., Norise, C., Faseyitan, O., Coslett, H.B., Turkeltaub, P.E., Hamilton, R.H., 2012. Finding the right words: transcranial magnetic stimulation improves discourse productivity in non-fluent aphasia after stroke. *Aphasiology* 26 (9), 1153–1168. <http://dx.doi.org/10.1080/02687038.2012.71031623280015>.
- Meinzer, M., Beeson, P.M., Cappa, S., Crinion, J., Kiran, S., Saur, D., Parrish, T., Crosson, B., Thompson, C.K., Neuroimaging in Aphasia Treatment Research Workshop, 2013. Neuroimaging in aphasia treatment research: consensus and practical guidelines for data analysis. *Neuroimage* 73, 215–224. <http://dx.doi.org/10.1016/j.neuroimage.2012.02.05822387474>.
- Meinzer, M., Elbert, T., Wienbruch, C., Djundja, D., Barthel, G., Rockstroh, B., 2004. Intensive language training enhances brain plasticity in chronic aphasia. *B.M.C. Biol.* 2, 20. <http://dx.doi.org/10.1186/1741-7007-2-201533104>.
- Meinzer, M., Flaisch, T., Breitenstein, C., Wienbruch, C., Elbert, T., Rockstroh, B., 2008. Functional re-recruitment of dysfunctional brain areas predicts language recovery in chronic aphasia. *Neuroimage* 39 (4), 2038–2046. <http://dx.doi.org/10.1016/j.neuroimage.2007.10.00818096407>.
- Meltzer, J.A., Braun, A.R., 2011. An EEG–MEG dissociation between online syntactic comprehension and post hoc reanalysis. *Front. Hum. Neurosci.* 5, 10. <http://dx.doi.org/10.3389/fnhum.2011.0001021331355>.
- Meltzer, J.A., Wagage, S., Ryder, J., Solomon, B., Braun, A.R., 2013. Adaptive significance of right hemisphere activation in aphasic language comprehension. *Neuropsychologia* 51 (7), 1248–1259. <http://dx.doi.org/10.1016/j.neuropsychologia.2013.03.00723566891>.
- Mühlau, M., Wohlschläger, A.M., Gaser, C., Valet, M., Weindl, A., Nunnemann, S., Peinemann, A., Etgen, T., Ilg, R., 2009. Voxel-based morphometry in individual patients: a pilot study in early Huntington disease. *A.J.N.R. Am. J. Neuroradiol.* 30 (3), 539–543. <http://dx.doi.org/10.3174/ajnr.A139019074546>.
- Musso, M., Weiller, C., Kiebel, S., Müller, S.P., Bülow, P., Rijntjes, M., 1999. Training-induced brain plasticity in aphasia. *Brain* 122 (9), 1781–1790. <http://dx.doi.org/10.1093/brain/122.9.178110468516>.
- Naeser, M.A., Martin, P.I., Nicholas, M., Baker, E.H., Seekins, H., Helm-Estabrooks, N., Cayer-Deade, C., Kobayashi, M., Theoret, H., Fregni, F., Tormos, J.M., Kurland, J., Doron, K.W., Pascual-Leone, A., 2005a. Improved naming after TMS treatments in a chronic, global aphasia patient – case report. *Neurocase* 11 (3), 182–193. <http://dx.doi.org/10.1080/1355479059094466316006338>.
- Naeser, M.A., Martin, P.I., Nicholas, M., Baker, E.H., Seekins, H., Kobayashi, M., Theoret, H., Fregni, F., Maria-Tormos, J., Kurland, J., Doron, K.W., Pascual-Leone, A., 2005b. Improved picture naming in chronic aphasia after TMS to part of right Broca's area: an open-protocol study. *Brain Lang.* 93 (1), 95–105. <http://dx.doi.org/10.1016/j.bandl.2004.08.00415766771>.
- Naeser, M.A., Martin, P.I., Treglia, E., Ho, M., Kaplan, E., Bashir, S., Hamilton, R., Coslett, H.B., Pascual-Leone, A., 2010. Research with rTMS in the treatment of aphasia. *Restor. Neurol. Neurosci.* 28 (4), 511–529. <http://dx.doi.org/10.3233/RNN-2010-055920714075>.
- Park, J., Kim, S., Kim, C., Cichocki, A., Kim, K., 2007. Multiscale entropy analysis of EEG from patients under different pathological conditions. *Fractals* 15 (04), 399–404. <http://dx.doi.org/10.1142/S0218348X07003691>.
- Phan, T.G., Donnan, G.A., Wright, P.M., Reutens, D.C., 2005. A digital map of middle cerebral artery infarcts associated with middle cerebral artery trunk and branch occlusion. *Stroke* 36 (5), 986–991. <http://dx.doi.org/10.1161/01.STR.0000163087.66828.e915817891>.
- Pincus, S.M., 1991. Approximate entropy as a measure of system complexity. *Proc. Natl. Acad. Sci. U. S. A.* 88 (6), 2297–2301.
- Raja Beharelle, A., Kovačević, N., McIntosh, A.R., Levine, B., 2012. Brain signal variability relates to stability of behavior after recovery from diffuse brain injury. *Neuroimage* 60 (2), 1528–1537. <http://dx.doi.org/10.1016/j.neuroimage.2012.01.03722261371>.
- Richman, J.S., Moorman, J.R., 2000. Physiological time-series analysis using approximate entropy and sample entropy. *Am. J. Physiol. Heart Circ. Physiol.* 278 (6), H2039–H2049.
- Ritter, P., Moosmann, M., Villringer, A., 2009. Rolandic alpha and beta EEG rhythms' strengths are inversely related to fMRI-BOLD signal in primary somatosensory and motor cortex. *Hum. Brain Mapp.* 30 (4), 1168–1187. <http://dx.doi.org/10.1002/hbm.2058518465747>.
- Rossini, P.M., Rossi, S., Babiloni, C., Polich, J., 2007. Clinical neurophysiology of aging brain: from normal aging to neurodegeneration. *Prog. Neurobiol.* 83 (6), 375–400. <http://dx.doi.org/10.1016/j.pneurobio.2007.07.01017870229>.
- Saur, D., Lange, R., Baumgaertner, A., Schracknepper, V., Willmes, K., Rijntjes, M., Weiller, C., 2006. Dynamics of language reorganization after stroke. *Brain* 129 (6), 1371–1384. <http://dx.doi.org/10.1093/brain/awl09016638796>.

- Singh, K.D., Barnes, G.R., Hillebrand, A., Forde, E.M., Williams, A.L., 2002. Task-related changes in cortical synchronization are spatially coincident with the hemodynamic response. *Neuroimage* 16 (1), 103–114. <http://dx.doi.org/10.1006/nimg.2001.105011969322>.
- Stam, C.J., 2005. Nonlinear dynamical analysis of EEG and MEG: review of an emerging field. *Clin. Neurophysiol.* 116 (10), 2266–2301. <http://dx.doi.org/10.1016/j.clinph.2005.06.01116115797>.
- Szaflarski, J.P., Vannest, J., Wu, S.W., DiFrancesco, M.W., Banks, C., Gilbert, D.L., 2011. Excitatory repetitive transcranial magnetic stimulation induces improvements in chronic post-stroke aphasia. *Med. Sci. Monit.* 17 (3), CR132–CR139. <http://dx.doi.org/10.12659/MSM.88144621358599>.
- Tecchio, F., Zappasodi, F., Pasqualetti, P., Tombini, M., Salustri, C., Oliviero, A., Pizzella, V., Vernieri, F., Rossini, P.M., 2005. Rhythmic brain activity at rest from rolandic areas in acute mono-hemispheric stroke: a magnetoencephalographic study. *Neuroimage* 28 (1), 72–83. <http://dx.doi.org/10.1016/j.neuroimage.2005.05.05116023869>.
- Tecchio, F., Zappasodi, F., Tombini, M., Oliviero, A., Pasqualetti, P., Vernieri, F., Ercolani, M., Pizzella, V., Rossini, P.M., 2006. Brain plasticity in recovery from stroke: an MEG assessment. *Neuroimage* 32 (3), 1326–1334. <http://dx.doi.org/10.1016/j.neuroimage.2006.05.00416806985>.
- Thiel, A., Habedank, B., Herholz, K., Kessler, J., Winhuisen, L., Haupt, W.F., Heiss, W.-D., 2006a. From the left to the right: how the brain compensates progressive loss of language function. *Brain Lang.* 98 (1), 57–65. <http://dx.doi.org/10.1016/j.bandl.2006.01.00716519926>.
- Thiel, A., Hartmann, A., Rubi-Fessen, I., Anglade, C., Kracht, L., Weiduschat, N., Kessler, J., Rommel, T., Heiss, W.-D., 2013. Effects of noninvasive brain stimulation on language networks and recovery in early poststroke aphasia. *Stroke* 44 (8), 2240–2246. <http://dx.doi.org/10.1161/STROKEAHA.111.00057423813984>.
- Thiel, A., Schumacher, B., Wienhard, K., Gairing, S., Kracht, L.W., Wagner, R., Haupt, W.F., Heiss, W.-D., 2006b. Direct demonstration of transcallosal disinhibition in language networks. *J. Cereb. Blood Flow Metab.* 26 (9), 1122–1127. <http://dx.doi.org/10.1038/sj.jcbfm.960035016757978>.
- Thompson, C.K., den Ouden, D.B., 2008. Neuroimaging and recovery of language in aphasia. *Curr. Neurol. Neurosci. Rep.* 8 (6), 475–483. <http://dx.doi.org/10.1007/s11910-008-0076-018957184>.
- Thulborn, K.R., Carpenter, P.A., Just, M.A., 1999. Plasticity of language-related brain function during recovery from stroke. *Stroke* 30 (4), 749–754. <http://dx.doi.org/10.1161/01.str.30.4.74910187873>.
- Tillema, J.M., Byars, A.W., Jacola, L.M., Schapiro, M.B., Schmithorst, V.J., Szaflarski, J.P., Holland, S.K., 2008. Cortical reorganization of language functioning following perinatal left MCA stroke. *Brain Lang.* 105 (2), 99–111. <http://dx.doi.org/10.1016/j.bandl.2007.07.12717905426>.
- Vrba, J., Robinson, S.E., 2001. Signal processing in magnetoencephalography. *Methods* 25 (2), 249–271. <http://dx.doi.org/10.1006/meth.2001.123811812209>.
- Waldowski, K., Seniów, J., Leśniak, M., Iwański, S., Członkowska, A., 2012. Effect of low-frequency repetitive transcranial magnetic stimulation on naming abilities in early-stroke aphasic patients: a prospective, randomized, double-blind sham-controlled study. *ScientificWorldJournal* 2012, 518568. <http://dx.doi.org/10.1100/2012/51856823213288>.
- Warburton, E., Price, C.J., Swinburn, K., Wise, R.J., 1999. Mechanisms of recovery from aphasia: evidence from positron emission tomography studies. *J. Neurol. Neurosurg. Psychiatry* 66 (2), 155–161. <http://dx.doi.org/10.1136/jnnp.66.2.15510071093>.
- Weiduschat, N., Thiel, A., Rubi-Fessen, I., Hartmann, A., Kessler, J., Merl, P., Kracht, L., Rommel, T., Heiss, W.D., 2011. Effects of repetitive transcranial magnetic stimulation in aphasic stroke: a randomized controlled pilot study. *Stroke* 42 (2), 409–415. <http://dx.doi.org/10.1161/STROKEAHA.110.59786421164121>.
- Westlake, K.P., Hinkley, L.B., Bucci, M., Guggisberg, A.G., Byl, N., Findlay, A.M., Henry, R.G., Nagarajan, S.S., 2012. Resting state alpha-band functional connectivity and recovery after stroke. *Exp. Neurol.* 237 (1), 160–169. <http://dx.doi.org/10.1016/j.jepneurol.2012.06.02022750324>.
- Wilson, K.R., O'Rourke, H., Wozniak, L.A., Kostopoulos, E., Marchand, Y., Newman, A.J., 2012. Changes in N400 topography following intensive speech language therapy for individuals with aphasia. *Brain Lang.* 123 (2), 94–103. <http://dx.doi.org/10.1016/j.bandl.2012.06.00522944529>.
- Winhuisen, L., Thiel, A., Schumacher, B., Kessler, J., Rudolf, J., Haupt, W.F., Heiss, W.D., 2007. The right inferior frontal gyrus and poststroke aphasia: a follow-up investigation. *Stroke* 38 (4), 1286–1292. <http://dx.doi.org/10.1161/01.STR.0000259632.04324.6c17322084>.
- Zappasodi, F., Tombini, M., Milazzo, D., Rossini, P.M., Tecchio, F., 2007. Delta dipole density and strength in acute monohemispheric stroke. *Neurosci. Lett.* 416 (3), 310–314. <http://dx.doi.org/10.1016/j.neulet.2007.02.01717321684>.